Journal of Alloys and Compounds 763 (2018) 257–266

Contents lists available at ScienceDirect

Journal of Alloys and Compounds

journal homepage: http://www.elsevier.com/locate/jalcom

PEG400-assisted synthesis of oxygen-incorporated MoS_2 ultrathin nanosheets supported on reduced graphene oxide for sodium ion batteries

Wen Chen [a, b], Wenwei Wu [b], Zhiyi Pan [a], Xuehang Wu [a, b, *], Huaxin Zhang [b]

[a] Guangxi Key Laboratory of Electrochemical Energy Materials, Collaborative Innovation Center of Renewable Energy Materials, Guangxi University, Nanning, Guangxi 530004, China
[b] School of Chemistry and Chemical Engineering, Guangxi University, Nanning, Guangxi 530004, China

ARTICLE INFO

Article history:
Received 10 February 2018
Received in revised form
24 May 2018
Accepted 25 May 2018
Available online 26 May 2018

Keywords:
Sodium ion batteries
MoS_2/rGO
Oxygen incorporation
Hydrothermal synthesis
Electrochemical performance
Structural analysis

ABSTRACT

Oxygen-incorporated MoS_2 (OI-MoS_2) ultrathin nanosheets have been successfully fabricated using a PEG400-assisted one-pot hydrothermal method. The role of polyethylene-glycol 400 (PEG400) in promoting the formation of long-range ordered single-phase OI-MoS_2 has not been investigated previously. In our study, we demonstrate that polyethylene-glycol 400 (PEG400) can act as a surfactant to reduce nanosheet aggregation. Furthermore, it can function as a structural modifier to regulate the degree of sulfidation and stabilize the oxygen-incorporated structure with larger interlayer spacing and higher intrinsic electronic conductivity for facilitating sodiation/de-sodiation reactions. A very low content of reduced graphene oxide (rGO) is enough to provide a highway for electron transport between adjacent OI-MoS_2 layers, and prevent OI-MoS_2 layers from stacking in the [002] direction. Enhanced electrochemical performance is observed in the OI-MoS_2/L-rGO nanosheets with carbonate-based electrolyte, delivering a discharge capacity of 462 mAh g^{-1} during the 2nd cycle with 89.1% capacity retention after 50 cycles.

1. Introduction

The rapid development of renewable energy is confronted with restrictions on energy storage and conversion technology in modern society. Lithium-ion batteries (LIBs) have dominated the advanced portable energy storage market due to the advantages of high energy density, high voltage, and long lifespans [1,2]. However, the limited and uneven distribution of lithium resources on the earth makes it difficult to support market growth from mobile electronic devices and electric vehicles to large-scale energy storage stations. Recently, sodium-ion batteries (SIBs) have been considered to be a better option compared to LIBs for stationary large-scale energy storage systems because of their high performance-to-price ratio [3–6]. Although SIBs and LIBs follow similar intercalation/de-intercalation chemistry, the Na^+ ion has a larger ionic radius (0.102 nm) than the Li^+ ion (0.076 nm), leading to the need for designing new-types of electrode materials.

Graphene-like two-dimensional (2D) materials have been developed into a new research branch in material fields [7–9]. Among them, molybdenum disulfide (MoS_2) has attracted increasing research interest in SIBs due to its tunable 2D interlayer space for accommodating relatively larger sodium ions [10–14]. When used as an electrode material for SIBs, layered MoS_2 material possesses a high theoretical capacity of 670 mAh g^{-1} in terms of the storage of four sodium ions per MoS_2. Despite this characteristic, the development of MoS_2 still faces two main limiting factors: first, MoS_2 has poor intrinsic electronic conductivity, including the directions along the (002) plane and perpendicular to the (002) plane. Second, MoS_2 usually suffers from large volume expansion and contraction during repeated sodiation/de-sodiation, leading to poor contact of the active material and rapid capacity fading [15–17].

Engineering the electronic structure and interface of MoS_2 by reasonably incorporating heteroatoms and molecules has been considered to be a promising strategy to overcome the intrinsic drawbacks of MoS_2 [18–21]. Xie et al. were the first to

* Corresponding author. Guangxi Key Laboratory of Electrochemical Energy Materials, Collaborative Innovation Center of Renewable Energy Materials, Guangxi University, Nanning, Guangxi 530004, China.
E-mail address: xhwu@gxu.edu.cn (X. Wu).

https://doi.org/10.1016/j.jallcom.2018.05.301
0925-8388/

systematically study the structure and catalytic performance of oxygen-incorporated MoS_2. Through first-principle calculations, they confirmed that oxygen incorporation in MoS_2 is an effective way to regulate the electronic structure for better intrinsic conductivity along the (002) plane [22]. In general, the incorporated oxygen may be derived from precursors, oxygen-containing surfactants/solvents, and preparation processes. The origin of the incorporated oxygen can exert a significant influence on the nature of MoS_2. When applied to SIBs, the problems, including the shuttle effect of intermediate sodium polysulfide in carbonate-based electrolytes should be taken into consideration. It is speculated that oxygen incorporation should be favorable to restrain the shuttle effect due to the reduction of the sulfur content. To date, the appropriate oxygen-incorporation method is still lacking and needs to be explored further. In addition, the electrochemical reversibility of SIBs can be further improved by optimizing interface properties with carbonaceous materials (such as organics, pyrolytic carbon, and graphene). Considerable efforts have been devoted to preparing MoS_2/carbon material composites to confine the volume changes, prevent the dissolution of active materials, and provide high electrical conductivity. For example, Dai et al. prepared superelastic 3D few-layer MoS_2/carbon framework heterogeneous electrodes ($MoS_2@C_F$) by a simple vacuum infiltration and heating process. The $MoS_2@C_F$ electrode displayed good cycling stability for sodium storage, with a high reversible capacity reaching up 360 mAh g^{-1} after 100 cycles at 0.1 A g^{-1} and an outstanding rate capability of 214 mAh g^{-1} at 2 A g^{-1} [23].

The short chain polymer, polyethylene-glycol 400 (PEG400), is generally utilized as a nonionic surfactant and preferentially adsorbs on the surface of growing nanoparticles during synthesis, facilitating anisotropic growth. Herein, we confirm that the PEG400 can act as a structural modifier to regulate the degree of sulfidation and confine oxygen removal, leading to the formation of oxygen-incorporated MoS_2 (OI-MoS_2) nanosheets with expanded interlayer spacing. The reduced graphene oxide (rGO) is utilized as a conducting matrix to grow and anchor MoS_2 nanosheets, thus reducing the stacking number of OI-MoS_2 layers and enhancing the mechanical strength and structural flexibility of nanosheets. The OI-MoS_2/L-rGO nanosheets exhibit better cycling stability than OI-MoS_2 without rGO addition and MoS_2/L-rGO without PEG400 addition. To elucidate the potential mechanism, the phase transitions of OI-MoS_2 and OI-MoS_2/L-rGO nanosheets during electrochemical sodiation/de-sodiation were characterized and compared by SEM and XRD techniques.

2. Experimental

2.1. Materials synthesis

Graphene oxide (GO) was prepared using a modified Hummers method from natural graphite powder as previously reported in the literatures [24,25]. The oxygen-incorporated MoS_2/reduced graphene oxide (rGO) nanosheets were synthesized with a one-pot hydrothermal method without further calcination. In a typical preparation process, 0.0128 g of GO was dispersed into deionized water (60 mL) by ultrasonication. Then, 1.936 g (8 mmol) of $Na_2MoO_4 \cdot 2H_2O$ and 20 mL of PEG-400 were added into the above solution and continually stirred for 15 min. Afterwards, 3.654 g (48 mmol) of thiourea ($(NH_2)_2CS$) was added dropwise under stirring. Finally, the solution was transferred into a Teflon-lined autoclave (100 mL) and the reaction temperature was maintained at 200 °C for 24 h. After cooling down to room temperature, the black precipitate was collected, washed with deionized water and ethanol several times, and then dried in a vacuum oven at 80 °C overnight to obtain the final product (OI-MoS_2/L-rGO, theoretical GO/MoS_2 ≈ 1 wt%). For comparison, similar procedures were also conducted to prepare the samples without GO addition (OI-MoS_2), with 0.0384 g of GO addition (OI-MoS_2/H-rGO, theoretical GO/MoS_2 ≈ 3 wt%), and without PEG400 addition (MoS_2 and MoS_2/L-rGO), respectively.

2.2. Materials characterization

XRD measurements were carried out using a powder X-ray diffractometer with Cu Kα radiation (Rigaku SmartLab, λ = 0.15406 nm). Sample morphologies and elemental distributions were characterized with a field emission scanning electron microscope (FESEM, SU8220) and a transmission electron microscope (TEM, Titan ETEM G^2). Raman spectroscopy measurements were carried out with a laser confocal micro-Raman spectrometer (LabRam HR800) with an excitation laser beam wavelength of 532 nm. XPS measurements were conducted with a PHI quantum 2000 scanning ESCA microprobe equipped with an Al Kα X-ray radiation source. Thermogravimetric analysis (TGA) was performed in air with a simultaneous thermal analyzer (Netzsch STA449-F5TAQ600). Before XRD measurements of electrode, coin cells were discharged/charged to the selected voltage states at 100 mA g^{-1}, and then disassembled in an argon-filled glovebox. The electrodes were taken out and cleaned with DMC to remove residual electrolytes. After the volatilization of DMC, the XRD patterns of the electrodes were collected.

2.3. Electrochemical measurements

Electrochemical tests were carried out using CR2032 coin-type cells assembled in an argon-filled glovebox ($O_2 < 0.1$ ppm, $H_2O < 0.1$ ppm). The working electrodes (14 mm in diameter) were prepared by mixing 80 wt% active material, 10 wt% Super P, and 10 wt% poly(vinylidene fluoride) (PVDF) binder in N-methyl-pyrrolidinone (NMP). The obtained homogeneous slurries were pasted

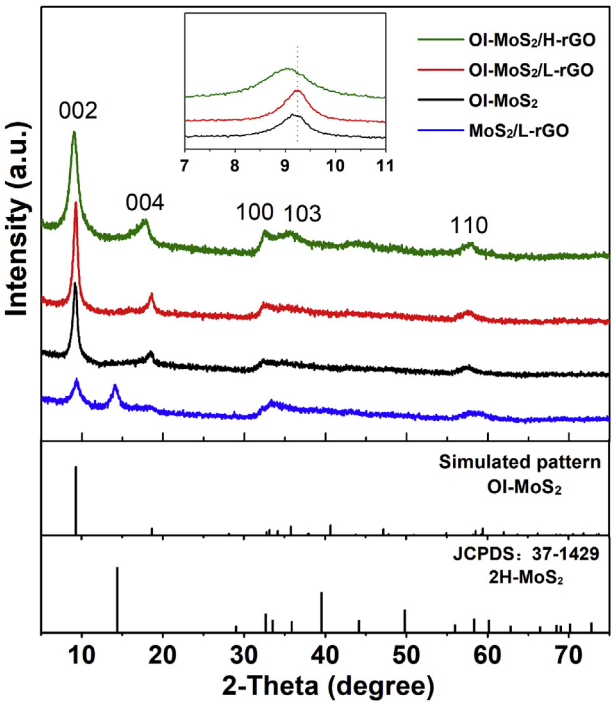

Fig. 1. (a) XRD patterns of the OI-MoS_2, OI-MoS_2/L-rGO, OI-MoS_2/H-rGO, and MoS_2/L-rGO nanosheets.